Mon. Not. R. Astron. Soc. **000**, 000–000 (0000) Printed 2 February 2008 (MN LATEX style file v2.2)

A Chandra View of the Multiple Merger In Abell 2744

Joshua C. Kempner⋆ and Laurence P. David
Harvard-Smithsonian Center for Astrophysics, 60 Garden St., Cambridge, MA 02138

Submitted 2003 October 7

ABSTRACT
We present a *Chandra* observation of the merging cluster of galaxies Abell 2744. The cluster shows strong evidence for an ongoing major merger which we believe to be responsible for the radio halo. X-ray emission and temperature maps of the cluster, combined with the spatial and redshift distribution of the galaxies, indicate a roughly north-south axis for the merger, with a significant velocity component along the line of sight. The merger is occurring at a very large velocity, with $\mathcal{M}$ = 2–3. In addition, there is a small merging subcluster toward the northwest, unrelated to the major merger, which shows evidence of a bow shock. A hydrodynamical analysis of the subcluster indicates a merger velocity corresponding to a Mach number of $\sim$1.2, consistent with a simple infall model. This infalling subcluster may also be re-exciting electrons in the radio halo. Its small Mach number lends support to turbulent reacceleration models for radio halo formation.

Key words: acceleration of particles — galaxies: clusters: individual (Abell 2744) — intergalactic medium — shock waves — turbulence — X-rays: galaxies: clusters

1 INTRODUCTION

One of the largest contributions that *Chandra* has made in its first few years of operation is in the study of merging clusters of galaxies. The unprecedented spatial resolution of the satellite has made possible the study of detailed physics of cluster interactions. Cold fronts—the sharp leading edges of moving cool cores of gas from clusters—along with their associated bow shocks have been imaged for the first time using *Chandra*. From these measurements, the dynamics of cluster mergers have been determined (e.g. A2142, Markevitch et al. 2000; A3667, Vikhlinin, Markevitch & Murray 2001a; 1E0657-56, Markevitch et al. 2002). These anlyses at high spatial resolution have also made it possible to demonstrate the suppression of conduction in clusters (Ettori & Fabian 2000; Vikhlinin et al. 2001b), to determine the dark matter distribution on small scales (Vikhlinin & Markevitch 2002). The resolution of *Chandra* has also provided the basis for the first measurement of a direct correlation between cluster merger shocks and diffuse radio emission in clusters (Markevitch & Vikhlinin 2001).

Abell 2744, also known as AC 118, is a rich (Abell richness class 3), luminous ($L_X(0.1-2.4\mathrm{keV}) = 22.05 \times 10^{44}$ erg sec^{-1}; Ebeling et al. 1996) cluster at moderate redshift ($z = 0.308$; Couch & Newell 1984). It hosts one of the most luminous known radio halos which covers the central 1.8 Mpc of the cluster, as well as a large radio relic at a distance of about 2 Mpc from the cluster center (Giovannini, Tordi & Feretti 1999, Govoni et al. 2001,?). Because of the presence of the radio halo and relic, Abell 2744 has been known to be undergoing a merger, but the details of the merger have been rather murky. Abell (1958) classified the spatial distribution of its galaxies as "regular," but it has no dominant bright galaxiy or galaxies so its Bautz-Morgan class is III (Bautz & Morgan 1970).

Observations of the cluster with *ROSAT* shed some light on the merger, showing the presence of a second peak in the X-ray brightness a little less than 1 Mpc to the northwest of the main peak. This second peak is much smaller and presumably much less massive than the main cluster, although it could have been stripped of much of its gas if it had already passed through the main cluster. The radio halo extends in the direction of this second peak, leading to the impression that the merger of the large main cluster and this smaller subcluster to the northwest is the cause of the radio halo, perhaps accelerating electrons via turbulence in its wake.

Our observation of the cluster with the higher resolution made possible by *Chandra* disproves this picture for the formation of the halo. While a merger does indeed appear to be resonsible for the radio halo, in fact it appears to be created by a merger between two subclusters with a small mass ratio, while the very small subcluster to the northwest is only beginning its descent into the potential of the two much larger subclusters and has only a small effect on the nonthermal emission.

We assume $H_0 = 50$ km s^{-1} Mpc^{-1} and $q_0 = 0.5$ throughout, for which $1'' = 5.58$ kpc and $d_L = 1970$ Mpc. All errors are quoted at 90% confidence unless otherwise stated.

⋆ jkempner@cfa.harvard.edu

2 OBSERVATION AND DATA REDUCTION

The data were taken on September 3, 2001 in a single observation of ∼24,800 seconds using the ACIS-S detector on *Chandra*, with the focus on the S3 chip. The data were taken in Very Faint (VF) mode, in order to allow for additional rejection of particle background events[1]. Very Faint mode data retains 5×5 pixel islands for each event, thereby making it possible to identify charged particle events that would appear to be valid photon events using the standard 3×3 pixel islands. This additional filtering of background events was performed, then the data were filtered on the standard *ASCA* grades 0, 2, 3, 4, and 6. Observations with *Chandra* are frequently affected by background flares where the background increases over the quienscent level. We checked for flares using the S-1 chip, which is quite sensitive to flares and is far enough away from the focal point of the detector to be essentially devoid of source photons. No flares occurred during our observation.

We used the period D blank sky background files for background correction. The background files were also screened using the VF mode filtering. We checked the quiescent background rate in our data by measuring the event rate on the S-3 chip in PHA channels 2500-3000, where the sensitivity to photons is extremely small, and compared it to the rate in the same PHA channels in the blank sky background files. The background level in our data was ∼19% below the nominal quiescent background level in the blank sky files, which include data from the beginning of period D when the quiescent level was slightly higher than the average for that period. We therefore corrected the background by the ratio of these quiescent rates when subtracting the background in our subsequent analysis. Despite this small correction, the background level in our data is consistent with the nominal quiescent level in PHA channels 2500-3000 at the date of the observation, to within the observed scatter[2] of the nominal level. Throughout this analysis, we used the calibration products in CALDB 2.17.

3 X-RAY PROPERTIES

3.1 X-ray Image

We show a raw *Chandra* image, binned into 2″pixels, in Figure 1. Figure 2 shows an adaptively smoothed version of the same image. The adaptively smoothed image was constructed using the CIAO tool *csmooth* with a minimum signal-to-noise of 3 and a maximum of 5. The blank sky background image and exposure map were both smoothed using the same kernel as for the source image. These smoothed images were then used to correct the source image. A mono-energetic exposure map was used, with energy at 0.8 keV—the peak of the emission in the central 2.′25 of the cluster.

The *Chandra* image shows two distinct components to the cluster: a large, irregular main cluster, and a much smaller subcluster to its northwest (see Figure 2). The main cluster, while fairly strongly peaked, does not fall off in surface brightness uniformly in all directions. Rather, it shows four "ridges" of emission extending to the north, northwest, southwest, and south. These ridges provide strong evidence, even in the absence of other information, that the cluster is out of hydrostatic equilibrium. All the ridges except the south ridge extend at least an arcminute out of the center, while the north rigde extends nearly two arcminutes. These three ridges also

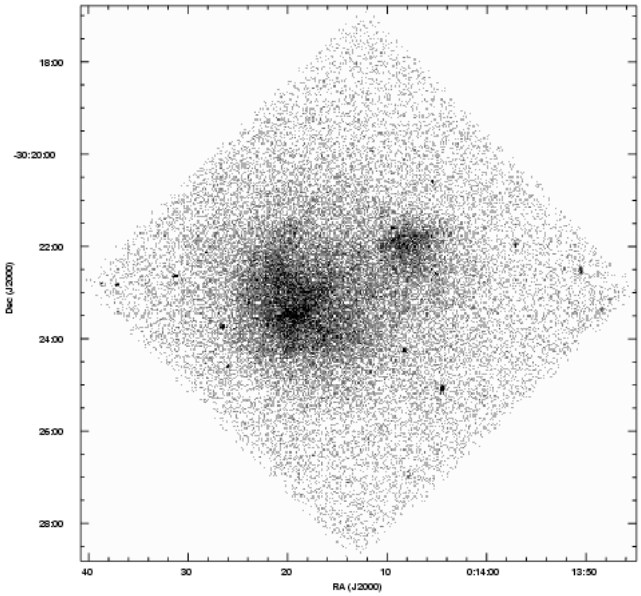

Figure 1. Raw *Chandra* image of Abell 2744. The entire S3 chip is shown.

show significant curvature, possibly suggesting internal angular momentum and turbulence within the main cluster. Even the ridges are not completely continuous: the south and north ridges have secondary surface brightness peaks away from the central peak of the main cluster, at roughly R.A. = $00^{\rm h}14^{\rm m}19.5^{\rm s}$, Dec. = $-30^\circ24^{\rm m}09^{\rm s}$ and R.A. = $00^{\rm h}14^{\rm m}20.5^{\rm s}$, Dec. = $-30^\circ22^{\rm m}45^{\rm s}$ respectively. These secondary peaks are clearly visible in Figure 2. We suspect these may be identified with the cool cores of merging subclusters, as we will discuss below.

At large radii, the substructure in the main cluster lessens. By a distance of ∼2.1′ from the cluster center, the surface brightness distribution falls off approximately uniformly in all directions except that of the northwest subcluster. In a β-model fit to a *ROSAT* PSPC image of the cluster, Govoni et al. (2001) find both an unusually large core radius of ∼640 kpc and an unusually steep value for β of 1.0. Their fit excludes the subcluster. The core they find encompasses exactly the "ridges" in the center of the main cluster as is evident from the *Chandra* data. The core radius they found may also have been broadened slightly by the large point spread function of *ROSAT*. We have fit a radial surface brightness profile, centered on the same point as that used in Govoni et al. (2001) (R.A. = $00^{\rm h}14^{\rm m}18.7^{\rm s}$, Dec. = $-30^\circ23^{\rm m}16^{\rm s}$), with a single-component β-model. We find the best-fit parameters to be $r_c = (474 \pm 33)$ kpc and $\beta = 0.79 \pm 0.06$ (1σ errors). The *Chandra* image shows that the cluster is too far from equilibrium, particularly in its core, for the parameters of the β-model fit to have any useful physical meaning.

About 2.7′ (∼900 kpc projected distance) to the northwest of the main cluster is a much smaller subcluster. At that distance, the subcluster is still well within the X-ray halo of the main cluster, which extends out to a radius of at least 11′ as detected by *ROSAT* (Govoni et al. 2001). The subcluster exhibits a sharp, curved eastern edge that is particularly distinct on its northeast side, with a surface brightness contrast across the edge of 1.7 ± 0.2 (1σ) and is hence very statistically significant.. From there, it fans out to the west, getting more diffuse with increasing distance from the east edge. These features indicate that the subcluster is moving from west to east, while its gas is swept back by ram pressure

[1] http://cxc.harvard.edu/cal/Links/Acis/acis/Cal_prods/vfbkgrnd/index.html
[2] http://asc.harvard.edu/contrib/maxim/bg/

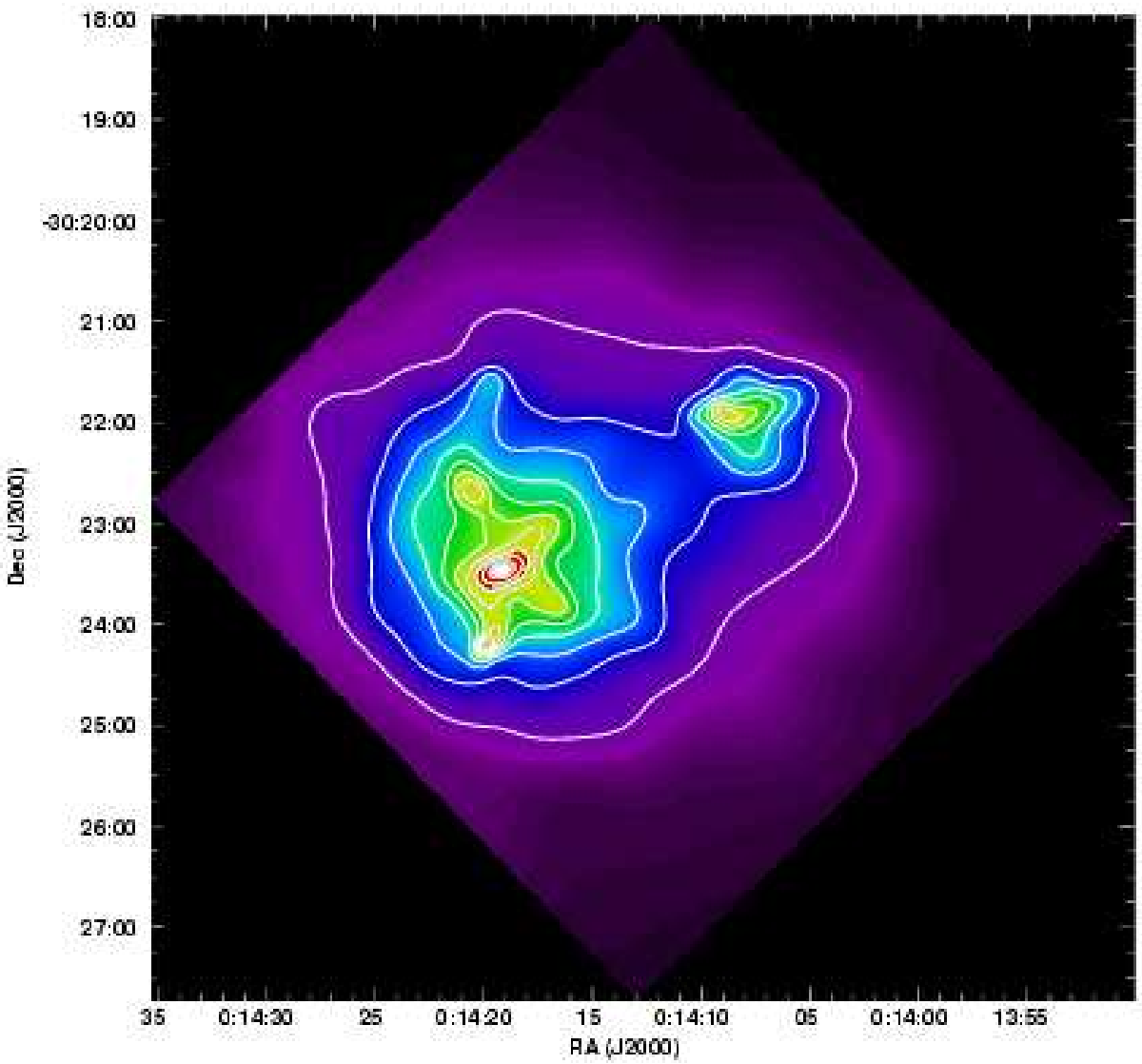

Figure 2. *(b)* Adaptively smoothed *Chandra* image of Abell 2744. The point sources were removed before smoothing. The color scale and contours are linearly spaced.

from the ICM of the main cluster. This characteristic "fan" shape of the subcluster is typical of smaller subclusters being ram pressure stripped by interaction with a larger cluster (cf. Kempner et al. 2002; Markevitch et al. 2002). As can be seen in Figure 1, the subcluster's fan of emission is brighter to one side (the north) than to the other. The contours in Figure 2 are also compressed on this side, indicating that the brightness falls off more steeply that it does on the south side of the subcluster. This morphology is similar to that of the south subcluster in Abell 85 (Kempner, Sarazin & Ricker 2002), which is quite similar in terms of both the mass ratio and the current separation of the constituent clusters. The "bullet" subcluster in 1E0657-56 (Markevitch et al. 2002) also shows this sort of asymmetry.

3.2 The Northwest Subcluster

As mentioned above, the raw image shows evidence that the northwest subcluster contains a "cold front" similar to those seen by *Chandra* in other clusters (e.g. A2142, Markevitch et al. 2000; A3667, Vikhlinin et al. 2001a; 1E0657-56, Markevitch et al. 2002). Also visible is a possible indication of a bow shock about 90 kpc ahead of the cold front (see Figure 3). Approximating the core as a sphere, the ratio of the stand-off distance of the shock to the radius of curvature of the cold core is determined only by the Mach number of the shock. Following Moekel (1949), this diagnostic indicates a Mach number of $\sim$1.2. The stand-off distance one measures, however, is highly sensitive to projection. That is, if the velocity of the subcluster has a significant line of sight component, we will have underestimated the stand-off distance, and thereby overestimated the Mach number. Futhermore, this method is exact only

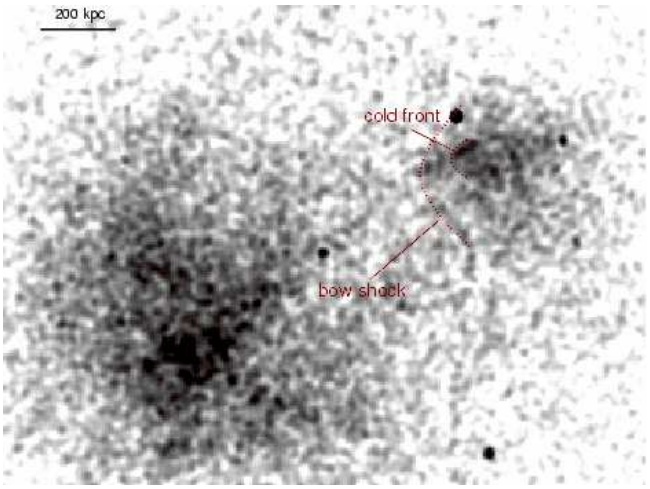

Figure 3. Gaussian smoothed, 0.3-6 keV image of Abell 2744. The cold front and bow shock are indicated in red.

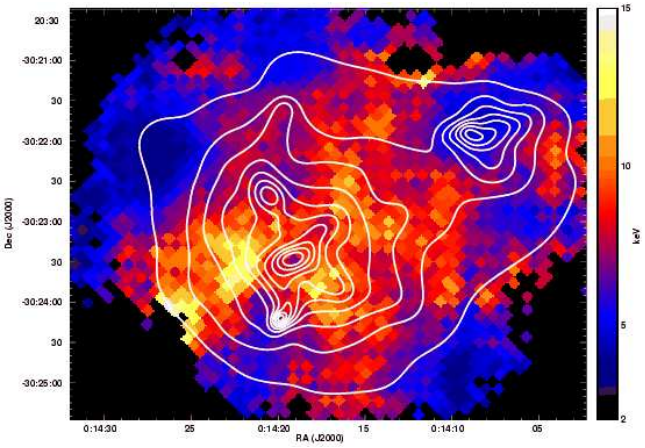

Figure 4. Temperature map of Abell 2744 made with adaptively binned spectra. The pixel size in the image is $6\farcs9$. The binning length ranges from $29\farcs3$ in high signal-to-noise areas to $63''$ in the outer parts of the cluster. Pixels with negative fractional error in the temperature of $> 15\%$ (90% confidence) have been masked out for clarity. Contours from Figure 2 are shown for reference.

for a perfect sphere, although the cold front is unlikely to deviate from this too much, at least on its leading edge.

The photon statistics are too poor to do a properly deprojected analysis of the electron densities across the cold front. There are, however, other methods for measuring the velocity of the subcluster. The surface brightness jump across the putative bow shock provides an approximate diagnostic of the subcluster's velocity. We approximate the square-root of the ratio of brightnesses on either side of the shock as the ratio of densities, that is, $(I_{X1}/I_{X2})^{1/2} \approx \rho_1/\rho_2$, which in turn is equal to the inverse of the shock compression. From this we determine the shock compression to be $C = 1.3 \pm 0.2$, which implies a Mach number of $\mathcal{M} = 1.2 \pm 0.2$ (both 1σ). From the image we can also roughly determine the opening angle of the Mach cone to be about 55–60 degrees, which implies a Mach number of 1.15–1.22. Thus, while the evidence of a bow shock is certainly not conclusive from the image, the consistency of the various diagnostics lends credence to the suggestion of a bow shock.

These various independent diagnostics for the velocity of the subcluster are all consistent with each other to within the measurement errors, all finding $\mathcal{M} \approx 1.2$. This is a good indication that the merger axis is not highly inclined to the plane of the sky. This is quite similar to the velocities found for the other merging subclusters mentioned above. As a sanity check, we also calculated the velocity for a collisionless point mass at the projected radius of the subcluster, falling from the turnaround radius into an isothermal potential with a mass of $2.70 \times 10^{15} M_\odot$ (Girardi & Mezzetti 2001). This simplistic model puts the velocity of the test particle at $\mathcal{M} = 1.2$ given the measured temperature of the main cluster of $9.3^{+4.9}_{-2.7}$ keV in the vicinity of the subcluster. This is also consistent with our measured velocity. We should note, however, that this velocity should be treated as an upper limit for this particular model, since projection effects would increase the actual separation of the subcluster and decrease its velocity. Furthermore, the fan-like shape of the subcluster indicates that the effects of ram pressure on the gaseous content of the subcluster are significant, further reducing its likely velocity compared to our simple model. Therefore, the model is only useful in setting the general scale of the subcluster's velocity, and for this purpose it is completely consistent with our data.

3.3 Temperature Structure

As might be expected from the complex structure in the X-ray image, the temperature structure in the cluster is quite complex as well. Figure 4 shows the temperature structure of the cluster in the higher signal-to-noise areas of the data. The temperature map was created using the adaptive binning algorithm described in Houck & Denicola (2000). The algorithm bins the data to a minimum of 800 counts in each extracted spectrum, while also minimizing the sizes of the extraction regions. The maximum allowed size of an extraction region was $63'' \times 63''$. Regions of this size with fewer than 800 counts were excluded from this analysis. The response matrices were generated on a 32×32 grid in chip coordinates. The ancillary responses were generated on a 16×16 grid in the coordinates of the binned output image. The systematic errors introduced by this binning are much smaller than the statistical errors in the temperature measurements. The systematic error is approximately 1%. Each pixel in the output map is $6\farcs9 \times 6\farcs9$. Each spectrum was corrected for background using a spectrum from a matching region in the blank sky background field discussed in §2. Regions containing point sources were eliminated from the source and background event lists. For clarity, we masked out all pixels in the final output image with negative fractional errors $> 15\%$ (90% confidence).

The final image shows several regions of 8–13 keV gas in the core of the cluster, surrounded by 6–7 keV gas. The 6–7 keV gas extends out to a radius of about 740 kpc, and even further in the direction of the northwest subcluster. Outside that radius, there is some evidence that the temperature drops even further, although the photon statistics are only good enough to make such a determination in one small area to the northeast. The upper limit on the temperature in this region is nowhere greater than 5 keV, whereas the lower limit at smaller radii is nowhere less than about 5.5 keV, so the temperature difference is real. However, deeper observations with a larger field of view are needed to confirm this drop in temperature at large radii, particularly since the temperature drop to the northeast could be a local phenomenon given the patchiness of the temperature structure throughout the cluster.

Two fingers of cooler gas extend into the center of the clus-

ter. The higher contrast one concides with the south surface brightness "ridge," while the lower contrast finger follows the north ridge. Both are oriented roughly north-south. In both cases these fingers of cool emission terminate with the bright peaks of emission in each ridge. The regions of hottest temperature in the core of the cluster correspond to the other surface brightness ridges. While ridges corresponding to the hotter gas, particularly the southwest and northwest ridges, are relatively sharp narrow features, the cooler ridges are somewhat broader. The north ridge is especially broad. We note, however, that the hottest region, just east of the cluster center, is not identified with any surface brightness enhancement. Another hot region, the finger of hot gas extending due south out of the cluster center, also is uncorrelated with a surface brightness enhancement.

The gas in the northwest subcluster, as discussed above, is significantly cooler than the ambient gas surrounding it.

4 GALAXY POPULATIONS AND DISTRIBUTION

Abell 2744 is a so-called Butcher-Oemler cluster (Butcher & Oemler 1978a,b, 1984), with an anomalously large fraction of blue galaxies compared to present-day clusters. The cluster has a marked deficiency of elliptical galaxies, a high percentage of spirals, and a normal percentage of S0 galaxies (Couch et al. 1998). Two large elliptical galaxies fall at the center of the galaxy population, just southeast of the peak of the X-ray emission, althought they are not significantly more luminous than the next brightest galaxies. The spatial distribution of the galaxies, in fact, is roughly centered on these two galaxies rather than on the peak of the X-ray gas, although neither of these two galaxies is morphologically identified as a cD (Couch et al. 1998).

To the northwest, in the direction of the subcluster, Andreon (2001) identifies a clump of galaxies which was associated with the X-ray subcluster. The X-ray emission from the subcluster is actually somewhat farther northwest than the concentration of galaxies. If the subcluster were falling straight into the main cluster, one would expected the collisionless galaxies to precede the collisional ICM as ram pressure from the interaction with the main cluster slows the descent of the subcluster into the main cluster potential. The morphology of the X-ray gas is largely in agreement with this interpretation, as we will discuss in greater detail in §5.

An extensive catalog of galaxy redshifts in Abell 2744 was compiled by Couch & Sharples (1987) and Couch et al. (1998). The distribution in redshift space of the combined sample from both these sources deviates significantly from a single Gaussian, as noted by Couch et al. (1998) for their subsample. With the addition of the sample from Couch & Sharples (1987), the distribution becomes murkier, but is still clearly non-Gaussian. While the sample is relatively small—only 72 galaxies—the distribution is noticeably bimodal. Girardi & Mezzetti (2001) find one peak at $z = 0.3014$ and the other peak at $z = 0.3148$. From this we see that the merger has a quite high velocity along the line of sight: $\Delta cz = 4000$ km s^{-1}. This unusually large merger velocity strongly suggests that the two subclusters are at or near their closest approach to one another. The extremely large line of sight component of the velocity also indicated that the merger is occurring largely, though not entirely, along the line of sight. As we will show in §5, a small transverse component to the merger is necessary to explain the data.

The further north of the two brightest ellipticals, at R.A. $= 00^{\rm h}14^{\rm m}20.6^{\rm s}$, Dec. $= -30^\circ24^{\rm m}00^{\rm s}$, has a redshift of $z = 0.30000 \pm 0.00033$ (Couch & Sharples 1987), which is at the peak of the bluer component of the distribution. The further south of the two bright ellipticals, at R.A. $= 00^{\rm h}14^{\rm m}22.0^{\rm s}$, Dec. $= -30^\circ24^{\rm m}20^{\rm s}$, has a redshift of $z = 0.31870 \pm 0.00033$ (Couch & Sharples 1987), which is near the peak of the redder component of the distribution. Girardi & Mezzetti (2001) also found that this combined set of galaxies was well fit by a bimodal distribution, with velocity dispersions of 1121^{+176}_{-88} km s^{-1} and 682^{+97}_{-75} km s^{-1}, respectively, for the bluer and redder components. These velocity dispersions correspond to $8.0^{+2.7}_{-1.2}$ keV and $3.0^{+0.9}_{-0.7}$ keV. Girardi & Mezzetti (2001) also fit these redshifts with a single Gaussian with a velocity dispersion that implies a virial temperature of $\sim$20 keV, more than twice the observed temperature through most of the cluster. They also note that the X-ray and lensing masses for the cluster are highly discrepant, which further suggests that the cluster is out of equilibrium and that a single cluster model for the galaxy velocities is therefore inappropriate.

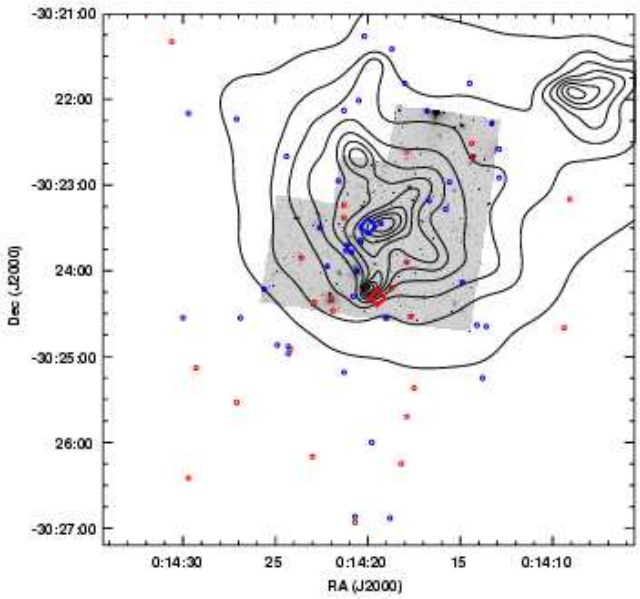

Figure 5. Spatial distribution of cluster members plotted on and around the HST image of the cluster. Blue circles are cluster galaxies with $z \leqslant 0.31$. Red circles are cluster galaxies with $z > 0.31$. The blue and red diamonds indicate the centroids of the respective samples of galaxies. Contours from Figure 2 are shown for reference.

The two populations in redshift space are also somewhat segregated on the sky. Figure 5 shows the spatial distribution of galaxies from the two populations, using $z = 0.31$ as the dividing line. The set of galaxies with measured redshifts is not uniformly sampled in all directions from the cluster center. In order to have a sample with equal north-south and east-west extent, we took only those galaxies within $2\farcm7$ of the center of the field used by Couch & Sharples (1987). This eliminated two galaxies with $z < 0.31$ and three with $z > 0.31$ from our sample. Like the two large ellipticals, the bluer galaxies tend to be segregated to the north, while the redder galaxies tend to be segregated to the south. The mean positions of the two populations, plotted as diamonds in Figure 5, illustrate the spatial segregation. A Kolmogorov-Smirnov test confirms this north-south segregation of the two populations with $> 90\%$ confidence. Thus, while the data are suggestive of a spatial segregation, they are by no means conclusive. We should also note that this sample of galaxies only covers the central 900 kpc, so any cluster galaxies at larger distances could alter the spatial distribution. We suspect that the true centroid of the approach-

ing galaxies, i.e. those with $z < 0.31$, would in fact change given a more complete sample of galaxies from a larger field, since the centroid we measure is so close to the center of the field and since they fill the field so completely. The receding galaxies, on the other hand, are a smaller population on the whole, so we have probably sampled a larger percentage of it within our field of view.

The only two systematic catalogues of redshifts for this cluster have concentrated on the central few arcminutes of the cluster and have not included the northwest subcluster. Consequently, it is not possible to determine the line of sight velocity of the northwest clump of galaxies relative to the main cluster, or even to confirm based on velocity that they are a distinct population belonging to a separately evolved cluster. A clue to determining their identity comes instead from their luminosity function. The faint end of the luminosity function of the northwest clump is flatter than that of the main cluster (Andreon 2001). This larger dwarf fraction is consistent with the galaxies having evolved in a less dense environment than that of the main cluster (Oemler 1974; Dressler 1978; Lopez-Cruz et al. 1997). We therefore confirm with some certainty the association of the northwest clump of galaxies with the subcluster detected in X-rays.

5 DISCUSSION

5.1 Dynamical History

The discussion that follows is an attempt to form a consistent picture for the dynamical history of the merger based on a confluence of the X-ray, optical, and radio data.

The X-ray brightness and temperature structure of the main cluster are extremely complex, particularly in the central 0.5 Mpc. The ridges in the X-ray brightness emission are largely correlated with features in the temperature structure. The cooler ridges are both oriented north-south, along the same axis as the centroids of the two galaxy populations discussed in §4. Both ridges show some curvature, and in opposite directions, consistent with being the wakes of the two subclusters if their interaction has a non-zero impact parameter. Futhermore, these two ridges show secondary surface brightness peaks, each about $0\farcm75$ (250 kpc) from the central peak of the main cluster, and each significantly cooler than the surrounding gas. These secondary brightness peaks with extended ridges of emission trailing away from the cluster center combined with the cold temperature of this gas relative to the rest of the cluster lead us to interpret the cooler ridges of bright emission to be the wakes of cooler gas from the cores of the respective subclusters, stripped by ram pressure through the earlier stages of the merger. Similarly, we interpret the two brightness peaks to be the cool cores of the respective subclusters. The fact that the cool wakes are visible at all demonstrates that the merger is not occurring entirely along the line of sight, but must have at least a small transverse component.

The hotter ridges are seen in the region where the gas should be the most strongly compressed ahead of the moving cool cores of the two subclusters. The velocity of the merger derived from the galaxy redshifts implies a Mach number for the merger of $\sim$2.6, using the temperature of the ambient cluster gas determined at the radius of the subcluster in §3.2 (9.3 keV). This Mach number is actually a lower limit since the temperature has probably been boosted by merger shocks by a factor of $\sim$1.5–2 (Ricker & Sarazin 2001) compared to its original value, and since the velocity derived from the galaxy redshifts excludes the transverse component of the velocity. Both of these factors would increase the actual strength of the shocks produced in the merger. In any case, the temperature jump across a $\mathcal{M} = 2.6$ merger shock would be a factor of 3. A fit to the northern cool core using a two-temperature MEKAL model (Kaastra 1992; Liedahl, Osterheld & Goldstein 1995), with the hotter temperature fixed to that of the surrounding hot gas, finds a temperature of the cool core of $4.6^{+3.0}_{-2.7}$ keV compared to a temperature of the surrounding hot gas of $10.6^{+4.6}_{-2.5}$. This temperature contrast is consistent with the predicted shock heating to within the (sizeable) errors. The two regions of hot gas which are not correlated with surface brightness enhancements (see §3.3) could be due to shocks that are largely perpendicular to the line of sight, and therefore do not appear as sharp features in the X-ray image.

The cool core to the north of the cluster center (the south-moving subcluster) is both larger and brighter than the south core. This suggests that it is the more massive of the two. This assertion may be corroborated by the galaxy populations: Girardi & Mezzetti (2001) found that the bluer population of galaxies, which has its centroid near the main X-ray peak, has a higher velocity dispersion than the redder population, which has its centroid further south. The mass ratio derived from the velocity dispersions is $\sim$4:1. Assuming that the gas has not yet decoupled from the dark matter and the galaxies, we would expect the positions of the cool cores and the galaxies to be correlated. This is probably a safe assumption since the merger appears to be at an earlier stage than, say, Abell 3667, in which the gas and dark matter are still coupled (Vikhlinin & Markevitch 2002). The data are inconclusive here, however. The projected separation of the south cool core from the centroid of the redder galaxies is a mere 60 kpc, but the separation of the centroid of the bluer galaxies from the north cool core is 250 kpc. These centroids are biased, however, by the relatively small area on the sky over which the galaxies have redshifts available in the literature. We therefore conclude that the spatial distributions of the galaxies are a poor test for determining the connection between the X-ray cores and the galaxy populations. The velocity dispersions are a more reliable test, however, and they appear to indicate that the north cool core has a negative line of sight velocity relative to the rest frame of the cluster, while the south core has a positive velocity along the line of sight in the same frame.

The cool wakes behind the cores, particularly to the north, give more insight into the dynamical history of the merger. The northern wake has significant curvature, indicating that the merger has a non-zero orbital angular momentum. Put another way, this shows that the merger is not head on, but has a non-zero impact parameter. Unfortunately, it is difficult to place even a meaningful lower limit on the value of the impact parameter since the cool wake of the south subcluster is too short to determine the transverse component of its direction of motion, and the direction implied by the wake of the north subcluster brings it into the south subcluster head on.

5.2 Radio Halo

The radio halo in Abell 2744 is one of the most luminous and most well studied (Govoni et al. 2001,?). The bulk of the diffuse radio emission is centered on the main cluster, with a radius of about $3'$. The cluster also hosts a radio relic at a projected distance of almost 2 Mpc from the cluster center. We will confine our discussion here to the halo, since the relic is too far from the ACIS focus for our data to contain many source photons from that region.

Figure 6 shows an image of the radio halo taken with the VLA at 20 cm, superimposed on the raw *Chandra* image. The offset between the peaks of the X-ray and radio images noted in Govoni et al. (2001) is probably not real, as the peak of the radio

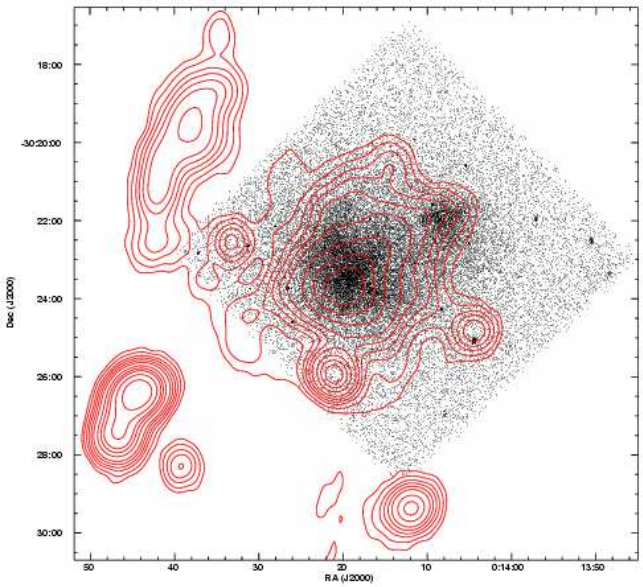

Figure 6. Raw *Chandra* image of Abell 2744 with contours of the radio halo image at 20 cm. The radio image has been smoothed with a restoring beam of $50'' \times 50''$(courtesy of F. Govoni). Three point sources around the edges of the halo are obvious; a fourth much fainter point source at $\mathrm{R.A.} = 00^{\mathrm{h}}14^{\mathrm{m}}14^{\mathrm{s}}$, $\mathrm{Dec} = 30^{\mathrm{h}}20^{\mathrm{m}}30^{\mathrm{s}}$ is responsible for the apparent extension of the halo to the north.

emission is resolved into several smaller peaks at slightly higher resolution than that of our Figure 6 (Govoni et al. 2001), the brightest of which is coincident with the X-ray brightness peak to within a few arcseconds.

The strong correlation between the X-ray and radio surface brightnesses that was found using lower resolution *ROSAT* data by Govoni et al. (2001) is also visible in our higher resolution data. We note some particularly interesting correlations: all the surface brightness ridges, both the cool ones and the hot ones, are correlated with brightness enhancements in the radio. The northwest subcluster is also correlated quite strongly with the radio halo. Also of note is a strong anti-correlation between the radio brightness ridge to the south of the cluster and the X-ray brightness. This feature in the radio image, however, follows exactly the temperature enhancement in the same region which we discussed above. If the high temperature of this gas is indeed due to a shock in that region, then the enhanced radio brightness there is most likely the result of current acceleration of cosmic ray electrons by the shock. Similarly, the other hot regions, which are more clearly indicative of shocks from their X-ray brightnesses, show enhanced radio emission. Given the large Mach number inferred above for the merger, the merger shocks should be strong enough to accelerate electrons to the energies necessary to produce the observed radio emission (Gabici & Blasi 2003).

The cool wake from the northern (south-moving) subcluster also shows enhanced radio emission. (The south wake shows no enhancement, but the bright radio point source in that part of the image makes it impossible to rule out enhanced diffuse emission.) Again, this probably indicates that cosmic ray electrons are currently be accelerated in these regions. No shocks are likely to exist in the cool stripped gas, so some other mechanism of particle acceleration is needed. Fujita, Takizawa & Sarazin (2003) demonstrated that turbulent resonant acceleration can generate the necessary electrons to produce radio halo emission, as long as a population of trans-relativistic electrons is already present. Such a population is clearly present, as indicated by the presence of large-scale diffuse radio emission. However, the velocity of the merger in Abell 2744 is so large that the timescale for the persistence of turbulence is small compared to the time required to re-accelerate these electrons if the radio emitting electrons have $\gamma \sim 10^4 - 10^5$. Electrons with $\gamma \gtrsim 10^3$ have radiative lifetimes of $\lesssim 10^9$ years (Sarazin 1999), while the turbulent timescale is at most $\sim 5 \times 10^8$ yr and perhaps even $\lesssim 10^8$ yr according to the simulations of Fujita et al. (2003), assuming the component subcluster masses derived by Girardi & Mezzetti (2001). It is also possible that the enhanced emission in the cool stripped gas is not due to current particle acceleration, but to a weaker magnetic field than is present in the rest of the cluster, thereby reducing the rate of synchrotron losses of the electrons. This could be the result of a stretching of the magnetic field as the gas is stripped from the core of the subcluster. Unfortunately, the actual mechanism for enhancing the radio emission cannot be distinguished using the currently available data. A direct detection of the magnetic field could be made from a spatially resolved detection of inverse Compton emission, which would enable us to determine if the enhancement is due to current particle acceleration or to a locally weaker magnetic field[3]. Either of these mechanisms, however, will have the same observable effect in the radio: the spectral index in the regions of enhanced emission should be flatter than that in the rest of the cluster because the electrons will have suffered fewer synchrotron losses. This should be easily measurable using lower frequency data with the same spatial resolution as the 20 cm data.

The northwest subcluster shows further evidence for particle acceleration, or more likely, re-acceleration. As can be seen in Figure 6, the radio halo emission extends to the northwest to completely cover the region of the northwest subcluster. Two possible scenarios can explain this extension of the radio halo to the northwewst.

The first scenario is simple shock acceleration from the observed bow shock ahead of the infalling subcluster. Other infalling subclusters with Mach numbers as small as that observed in Abell 2744 do not show any evidence of diffuse radio emission (e.g. Abell 85, Kempner et al. 2002). Gabici & Blasi (2003) demonstrated that even in the case of a cluster with a pre-existing population of suprathermal electrons, weak shocks such as the bow shock in question produce an energy spectrum of accelerated electrons that is too steep to explain the observed radio emission. This predicted lack of radio emission is consistent with observations of other infalling subclusters, and thus we find it unlikely that the bow shock in Abell 2744 is responsible for producing the observed radio emission.

The second scenario assumes that a pool of "seed" electrons at mildly relativistic energies exists, which can be accelerated to the necessary energies. A population of suprathermal electrons does indeed exist in much of the cluster, as the existence of the radio halo demonstrates, but its presence at radii beyond the edge of the 20 cm radio emission is less obvious. As has been seen in other clusters with radio halos, the halos' spectra steepen with radius, so the halos appear much larger at lower frequencies (e.g. Coma,

[3] This assumes both that variations in the magnetic field strength are resolved and that the relativistic electrons are distributed similarly to the field lines. Coherent structures over 10s of kiloparsecs observed in Faraday rotation maps (e.g. Eilek & Owen 2002) give some hope for the former, but the latter remains a tenuous assumption.

Giovannini et al. 1993; Deiss et al. 1997; for a theoretical explanation, see Brunetti et al. 2001). Therefore it is quite likely that a population of electrons exists at the radius of the infalling subcluster, the energies of which are too low to emit synchrotron radiation at 20 cm. Unfortunately, the lack of data at longer wavelengths for Abell 2744 makes it impossible to verify this assumption at present. As long as 2744 is not unique, it should have the necessary seed electrons at the radius of the subcluster. The model of Fujita et al. (2003), discussed above, is most efficient at re-accelerating electrons in exactly this sort of situation, i.e. a large mass ratio merger at an early stage where the merger velocity is still small. Thus, turbulent re-acceleration of seed electrons could also account for the extent of the halo across the subcluster. In principle, these two scenarios could be distinguished by detailed spectral index maps of the halo in the vicinity of the subcluster. In the first scenario, the halo would show a spectral index gradient from the flattest part near the bow shock, where the electrons are currently being accelerated, to the wake of the subcluster, where the electrons would be passively aging. The second scenario would create a more uniform spectral index, since electrons are being accelerated throughout the wake of the subcluster.

6 SUMMARY

We have presented a new *Chandra* observation of Abell 2744 which shows that the main cluster is in a highly disturbed state. Temperature and surface brightness variations are observed on all scales along with the cool cores of the constituent subclusters amid strong ($\mathcal{M} \gtrsim 2$) merger shocks. The bi-modal distribution of the member galaxies and the morphology of the radio halo provide further evidence that the cluster is undergoing a major merger. We propose a dynamical scenario for the merger which involves a merger of two subclusters with a mass ratio near unity and a non-zero impact parameter. A significant component of the merger axis is estimated to be along the line of sight.

We have also studied the small merging subcluster to the northwest and estimate an infall velocity of $\mathcal{M} \sim 1.2$. We also demonstrate that this subcluster is not responsible for the bulk of the disturbed nature of the ICM of the main cluster. Nonetheless, its effect on the cluster's extremely powerful radio halo is significant, at least in the immediate vicinity of the subcluster. We conclude that turbulent re-acceleration of electrons in the wake of the subcluster is probably responsible for the extension of the radio halo across the subcluster. Future radio observations of the subcluster at lower frequencies should be able to determined or strongly constrain the formation mechanism of the radio halo.

Acknowledgments
We thank Federica Govoni for the deep radio image of the cluster. Support for this work was provided by the National Aeronautics and Space Administration through *Chandra* Award Number GO2-3171X issued by the *Chandra* X-ray Observatory Center, which is operated by the Smithsonian Astrophysical Observatory for and on behalf of NASA under contract NAS8-39073.

REFERENCES

Abell G. O., 1958, ApJS, 3, 211
Andreon S., 2001, ApJ, 547, 623
Bautz L. P., Morgan W. W., 1970, ApJL, 162, L149
Brunetti G., Setti G., Feretti L., Giovannini G., 2001, MNRAS, 320, 365
Butcher H., Oemler A., 1978a, ApJ, 219, 18
Butcher H., Oemler A., 1978b, ApJ, 226, 559
Butcher H., Oemler A., 1984, ApJ, 285, 426
Couch W. J., Barger A. J., Smail I., Ellis R. S., Sharples R. M., 1998, ApJ, 497, 188
Couch W. J., Newell E. B., 1984, ApJS, 56, 143
Couch W. J., Sharples R. M., 1987, MNRAS, 229, 423
Deiss B. M., Reich W., Lesch H., Wielebinski R., 1997, A&A, 321, 55
Dressler A., 1978, ApJ, 223, 765
Ebeling H., Voges W., Bohringer H., Edge A. C., Huchra J. P., Briel U. G., 1996, MNRAS, 281, 799
Eilek J. A., Owen F. N., 2002, ApJ, 567, 202
Ettori S., Fabian A. C., 2000, MNRAS, 317, L57
Fujita Y., Takizawa M., Sarazin C. L., 2003, ApJ, 584, 190
Gabici S., Blasi P., 2003, ApJ, 583, 695
Giovannini G., Feretti L., Venturi T., Kim K.-T., Kronberg P. P., 1993, ApJ, 406, 399
Giovannini G., Tordi M., Feretti L., 1999, New Astronomy, 4, 141
Girardi M., Mezzetti M., 2001, ApJ, 548, 79
Govoni F., Enßlin T. A., Feretti L., Giovannini G., 2001, A&A, 369, 441
Govoni F., Feretti L., Giovannini G., Böhringer H., Reiprich T. H., Murgia M., 2001, A&A, 376, 803
Houck J. C., Denicola L. A., 2000, in ASP Conf. Ser. 216: Astronomical Data Analysis Software and Systems IX ISIS: An Interactive Spectral Interpretation System for High Resolution X-Ray Spectroscopy. ASP, San Francisco, p. 591
Kaastra J. S., 1992, Technical report, An X-Ray Spectral Code for Optically Thin Plasmas
Kempner J. C., Sarazin C. L., Ricker P. M., 2002, ApJ, 579, 236
Liedahl D. A., Osterheld A. L., Goldstein W. H., 1995, ApJL, 438, 115
Lopez-Cruz O., Yee H. K. C., Brown J. P., Jones C., Forman W., 1997, ApJL, 475, L97
Markevitch M., Gonzalez A. H., David L., Vikhlinin A., Murray S., Forman W., Jones C., Tucker W., 2002, ApJL, 567, L27
Markevitch M., Ponman T. J., Nulsen P. E. J., Bautz M. W., Burke D. J., David L. P., Davis D., Donnelly R. H., Forman W. R., Jones C., Kaastra J., Kellogg E., Kim D.-W., Kolodziejczak J., Mazzotta P., Pagliaro A., Patel S., Van Speybroeck L., Vikhlinin A., Vrtilek J., Wise M., Zhao P., 2000, ApJ, 541, 542
Markevitch M., Vikhlinin A., 2001, ApJ, 563, 95
Moekel W. E., , 1949, Approximate Method for Predicting Forms and Location of Detached Shock Waves Ahead of Plane or Axially Symmetric Bodies, NACA Technical Note 1921
Oemler A. J., 1974, ApJ, 194, 1
Ricker P. M., Sarazin C. L., 2001, ApJ, 561, 621
Sarazin C. L., 1999, ApJ, 520, 529
Vikhlinin A., Markevitch M., Murray S. S., 2001a, ApJ, 551, 160
Vikhlinin A., Markevitch M., Murray S. S., 2001b, ApJL, 549, L47
Vikhlinin A. A., Markevitch M. L., 2002, Astronomy Letters, 28, 508